

LA-UR-97-4002


Title:

**FRAGMENTATION AND ABLATION  
DURING ENTRY**

Author(s):

Gregory H. Canavan, P-DO

**RECEIVED  
FEB 02 1998  
OSTI**

DISTRIBUTION OF THIS DOCUMENT IS UNLIMITED 

Submitted to:

For discussions outside the Laboratory

**MASTER**

Date: September 1997

**Los Alamos**  
NATIONAL LABORATORY



Los Alamos National Laboratory, an affirmative action/equal opportunity employer, is operated by the University of California for the U.S. Department of Energy under contract W-7405-ENG-36. By acceptance of this article, the publisher recognizes that the U.S. Government retains a nonexclusive, royalty-free license to publish or reproduce the published form of this contribution, or to allow others to do so, for U.S. Government purposes. The Los Alamos National Laboratory requests that the publisher identify this article as work performed under the auspices of the U.S. Department of Energy.

Form No. 836 R5  
ST 2629 10/91

### **DISCLAIMER**

This report was prepared as an account of work sponsored by an agency of the United States Government. Neither the United States Government nor any agency thereof, nor any of their employees, makes any warranty, express or implied, or assumes any legal liability or responsibility for the accuracy, completeness, or usefulness of any information, apparatus, product, or process disclosed, or represents that its use would not infringe privately owned rights. Reference herein to any specific commercial product, process, or service by trade name, trademark, manufacturer, or otherwise does not necessarily constitute or imply its endorsement, recommendation, or favoring by the United States Government or any agency thereof. The views and opinions of authors expressed herein do not necessarily state or reflect those of the United States Government or any agency thereof.

## **DISCLAIMER**

**Portions of this document may be illegible electronic image products. Images are produced from the best available original document.**

## FRAGMENTATION AND ABLATION DURING ENTRY

Gregory H. Canavan

Objects that both fragment and ablate during entry can be treated by an extension to the previous separate models. The model agrees with numerical calculations and retains the invertibility desired for the interpretation of experimental data.

This note discusses objects that both fragment and ablate during entry, using the results of previous reports to describe the velocity, pressure, and fragmentation of entering objects. It shows that the mechanisms used there to describe the breakup of non-ablating objects during deceleration remain valid for most ablating objects. It treats coupled fragmentation and ablation during entry, building on earlier models that separately discuss the entry of objects that are hard, whose high heat of ablation permits little erosion, and those who are strong whose strength prevents fragmentation, which are discussed in "Radiation from Hard Objects,"<sup>1</sup> "Deceleration and Radiation of Strong, Hard, Asteroids During Atmospheric Impact,"<sup>2</sup> and "Meteor Signature Interpretation."<sup>3</sup>

This note provides a more detailed treatment of the further breakup and separation of fragments during descent. It replaces the constraint on mass per unit area used earlier to determine the altitude and magnitude of peak power radiation with a detailed analytic solution of deceleration. Model predictions are shown to be in agreement with the key features of numerical calculations of deceleration. The model equations are solved for the altitudes of maximum radiation, which agree with numerical integrations. The model is inverted analytically to infer object size and speed from measurements of peak power and altitude to provide a complete model for the approximate inversion of meteor data.

**Ablation.** An earlier note discusses fragmentation without ablation during entry.<sup>4</sup> For objects that ablate it is necessary to incorporate the fact that its area  $A$  decreases as material is eroded. That can be done by complementing the equation for the conservation of momentum under drag

$$Mdv/dt = -C_pAV^2, \quad (1)$$

with an equation for the rate of change of mass due to ablation

$$QdM/dt = -J_pAV^3, \quad (2)$$

where  $Q$  is the heat of vaporization, which is given for various object types in Table 1, and  $J = 0.1$  is a heat transport coefficient.<sup>5</sup> Taking the ratio of Eqs. (1) to (2) and integrating produces

$$M = M_0 \exp[-K(1 - v^2)], \quad (3)$$

where  $M_0$  and  $V_0$  are the object's initial mass and velocity,  $v = V/V_0$ , and  $K$  is a parameter

$$K = JV_0^2/2CQ. \quad (4)$$

Equation (3) indicates that the object's relative mass at any altitude is determined by  $K$  and  $v$ . For  $K$  constant, it can be used to evaluate the current area  $A \approx D^2 \approx D_0^2(M/M_0)^{2/3} = D_0^2m^{2/3}$ , which on substitution into Eq. (1) produces an equation in  $V$  only. The ablation parameter  $K$  for a typical initial velocity of  $V_0 = 15$  km/s is shown in Table I

Table 1. Approximate meteor parameters.

type	density(kg/m <sup>3</sup> )	Q(J/kg)	S(N/m <sup>2</sup> )	C	I	K
iron	8000	8x10 <sup>6</sup>	10 <sup>8</sup>	2	0.1	0.70
stone	3500	8x10 <sup>6</sup>	10 <sup>7</sup>	2	0.1	0.70
carbon	2200	5x10 <sup>6</sup>	10 <sup>6</sup>	2	0.1	1.13
cometary	1000	2.5x10 <sup>6</sup>	10 <sup>5</sup>	2	0.1	2.25

For iron,  $K \approx 0.7$ , so that even when the velocity drops 10% below  $V_0$ , the objects mass only falls  $\approx 1 - e^{-0.7 \times 0.8} \approx 40\%$ , and the diameter  $\approx 10\%$ . Weak ablation, i.e.,  $V_0^2/Q$  small, gives  $K \ll 1$  even for large  $V_0^2$ , which means  $M/M_0$  falls slowly with velocity. The limit of  $V_0^2/Q \approx 0$  is the non-ablative limit treated in the earlier papers cited above. Conversely, cometary material gives  $K \approx 2.25$ , which would reduce mass  $\approx 1 - e^{-2.25 \times 0.8} \approx 90\%$  as the velocity fell 10%. Strong ablation, i.e.,  $V_0^2/Q$  large, gives  $K \gg 1$ , so that  $M/M_0$  falls rapidly with  $v$ , which corresponds to the limit of mechanically strong but thermally soft objects. Stony objects have a value of  $Q$  similar to that of iron, so they ablate similarly. Carbonaceous objects are intermediate between stony and cometary objects in  $Q$  and in the effects of ablation.

**Fragmentation conditions.** The earlier note established the rough criteria for breakup that the pressure on the front of the object, reach the mechanical strength of the object,  $S$ . The ram pressure is approximately

$$p \approx C\rho V^2, \quad (5)$$

As the object descends, the density increases but its velocity decreases, so the pressure has a maximum at some intermediate altitude. An approximate solution to Eqs. (1) and (2) is

$$V \approx V_0 e^{-\rho H/\beta}, \quad (6)$$

where  $\beta$  is the areal density or ballistic coefficient of an object of mass  $M$ , area  $A$ , and density  $\rho_a$

$$\beta = M/A \approx (4\pi/3)\rho_a(D/2)^3/\pi(D/2)^2 \approx 0.7\rho_a D. \quad (7)$$

Figure 1 compares the velocity from Eq. (6) with that from a direct numerical integration of Eqs. (1) and (2) for the vertical entry of a stony object at 15 km/s. The numerical solution shown by solid squares shows sharp deceleration below about 25 km. The approximate solution, which is quite close, is shown by solid diamonds. The open squares show the velocity that results from

using the time dependent value of  $\beta$  for the eroding object in Eq. (6). That approximation significantly overestimates the deceleration of the object because it applies the reduced density to the object's whole trajectory. In general, the solution using the initial  $\beta$  is more accurate before fragmentation, although it is necessary to use the rapidly decreasing  $\beta$  from breakup after fragmentation.

This level of agreement between the numerical and approximate velocity is obtained for a range of values of  $\beta$ ,  $V_0$ , and  $Q$ . Because the initial  $\beta$  gives an adequate approximation to  $V$ , it is not necessary to include the indirect effect of  $Q$  through  $\beta$  in estimating  $V$ .

The corresponding approximation to the pressure is

$$p \approx C\rho V^2 \approx C\rho V_0^2 e^{-2\rho H/\beta}, \quad (8)$$

which is compared to the numerical solution of Eqs. (1) and (2) in Fig. 2. The agreement is almost exact. This level of agreement again holds for a range of  $\beta$ ,  $V_0$ , and  $Q$ , so it is not necessary to include the indirect effect of ablation through the effect of decreasing area on  $\beta$  to determine the dynamic pressure accurately. Because of this insensitivity of fracture to  $Q$ , the treatment of "Fragmentation of Weak Non-Ablating Objects During Entry" in the earlier paper is not changed to first order. That is not only a convenience, it means it is not necessary to review the full process of fragmentation again. Instead, Figs. 1-3 of "Fragmentation of Weak Non-Ablating Objects" can be used as they are to describe the early phases of entry.

Because of this insensitivity of fracture to  $Q$ , it is also possible to use the initial value of  $\beta$  in differentiating  $p$  with respect to  $\rho$  to find the density,  $\rho_m = \beta/2H$ , at which pressure is maximum,

$$\rho_m \approx CV_0^2 \beta/2H, \quad (9)$$

For the parameters of Fig. 2,  $\rho_m = \beta/2H \approx 0.7 \times 3000 \text{ kg/m}^3 \times 0.5 \text{ m} / 2 \times 7000 \text{ m} \approx 0.075 \text{ kg/m}^3$ , so  $z_m \approx 20 \text{ km}$ , as seen. If  $\rho_m$  is less than the maximum stress,  $S$ , the object does not fracture, it merely ablates during entry, as treated in earlier reports. If  $\rho_m$  exceeds  $S$ , it fractures. The case where it  $\rho_m$  exceeds  $S$ , but the object has a very high heat of vaporization was treated in the previous report.<sup>6</sup> The case where it fragments and then subsequently ablates is treated below.

**After fragmentation**, conditions change more rapidly. Figure 3 shows the power radiated as a function of altitude (measured from 20 km for ease of plotting) from 1 m objects at 15 km/s vertical entry with heats of vaporization ranging from 1 to 16 MJ/kg, which more than span the values in Table I. Perhaps the most important observation is the simplest one: fragmentation has a major impact on the flow parameters absent fragmentation, but ablation has only a factor of two impact on those from fragmentation. That is, in the absence of fragmentation, the power curves would extend over one or more scale heights at much lower altitudes. With fragmentation, the power radiation is compressed into 1 km in altitude for the

lowest  $Q$  and only about 2 km for the highest. Conversely, given fragmentation, the full range of  $Q$  only changes the peak radiation rate by about a factor of two, and the width by a like amount.

Ablation does, however, have a noticeable impact on post-fragmentation conditions. Figure 4 shows the velocity as a function of altitude (from 20 km) for 1 m objects with heats of vaporization from 1 to 16 MJ/kg incident vertically at 15 km/s. All experience significant deceleration by 24-25 km and are essentially stopped by 23-24.5 km. While these differences are of interest, they would not be detectable with the rough altitude and time resolution of current sensors. Comparing Figs. 4 and 3 shows that for each value of  $Q$ , the velocity has only decreased about 20% from its initial value at the time of peak radiated power, which would be difficult to detect kinematically.

Figure 5 shows the mass as a function of altitude (from 20 km) for 1 m objects with 1 to 16 MJ/kg heats of vaporization from incident vertically at 15 km/s. All experience significant erosion by 24-26 km. Those with  $Q < 2$  MJ/kg are essentially eroded away by 25 km. Stone and iron objects would be eroded by about a factor of two. Stronger objects would be eroded little. These differences are significant in predicting the amount of meteoroids that might be found, they would not be detectable with current sensors, which are primarily sensitive to light emission. Comparing Figs. 5 and 3 shows that for each  $Q$ , the mass has decreased by less than a factor of two from its initial value at the time of peak radiated power, which is within the range of validity of the scaling models used below.

Figures 3, 4, and 5—together with the treatment of fragmentation presented in "Fragmentation of Weak Non-Ablating Objects"—provide the formal basis for predicting the optical observables from objects of various sizes and speeds. The previous paper also discusses the scaling of radiated power  $P \propto (DV)^3$  for non-ablating objects. The remainder of this paper largely discusses how that scaling—and its inversion—are modified for strongly ablating objects. However, Fig. 3 already indicates the principal result: ablation makes factor of two modifications to the basic parameters set by fragmentation.

**Analysis.** Before fragmentation, the velocity changes relatively little, which permits replacing  $v = V/V_0$  in Eq. (6) by

$$v \approx e^{-\rho H/\beta} \approx 1 - \rho H/\beta. \quad (10)$$

which reduces Eq. (3) to

$$m = \exp[-K(1 - v^2)] \approx \exp[-K(1 - \{1 - 2\rho H/\beta_0\})] \approx e^{-2K\rho H/\beta_0} \approx v^2 K. \quad (11)$$

Figures 4 and 5 show that these approximations for  $v$  and  $m$  are not accurate after fragmentation. However, the result in Eq. (3), that the relative mass is a direct function of the relative velocity, holds whether or not the object fragments. Thus, it is valid throughout the fragmentation process, if a replacement for the  $v$  of Eq. (10) can be found.

If the object fragments, that increases its total effective area, which increases drag, which causes the fragments to decelerate faster. As long as the pressure on a fragment remains larger than its strength, it will fragment, which increases the total area still further. That process can proceed through several generations until the fragments move too far apart to share a common shock or are decelerated enough to reduce the pressure below their material strength, which stops the cascade process and allows the fragments to descend as individual objects.

This cascade process can be modeled approximately. After breakup the fragments move apart at an approximate transverse speed<sup>7</sup>

$$V_t \approx k\sqrt{(\rho_f/\rho_a)} V, \quad (12)$$

where  $\rho_f$  is the density at the breakup altitude and  $k$  is a constant on the order of unity. For stony objects with  $\rho_a \approx 3,000 \text{ kg/m}^3$  that breakup at about 30 km, or  $\rho_f \approx 0.01 \text{ kg/m}^3$ ,  $\sqrt{(\rho_f/\rho_a)} \approx 0.002$ , so  $V_t \approx 0.002 V \approx 40 \text{ m/s}$ . Thus, in descending a distance  $h$ , the fragments expand to a diameter

$$D_f \approx V_t h/V \approx k\sqrt{(\rho_f/\rho_a)} h, \quad (13)$$

and area

$$A \approx D_f^2 \approx k^2(\rho_f/\rho_a) h^2, \quad (14)$$

which can be substituted into Eq. (1). However, to separate Eqs. (1) and (2) it is necessary to make the further approximation that the mass does not change rapidly during cascade expansion. That is justified by Fig. 5, which shows that the mass typically falls by less than a factor of two during deceleration. The one additional approximation is that the density does not vary rapidly during deceleration. Figure 4 shows that deceleration typically occurs over a distance of 2-3 km, during which the density increases by less than a factor of two. With these approximations, which are discussed further below, Eq. (1) reduces to

$$M dV/dt = -C\rho_f (D + V_t t)^2 V^2, \quad (15)$$

whose solution is

$$V_a = 1/\{[(D + V_t t)^3 - D^3]NC\rho_f/(3MV_t) + 1/V_o\}, \quad (16)$$

where  $V_o$  is the initial velocity and  $N$  is a parameter inserted to account for the averaging over density and mass. Figure 6 compares the numerical solution of Eqs. (1) and (2) with the results of Eq. (16) for the fragmentation of a 1 m object at 28 km. The analytic plots are shown for  $N = 0.25$  and  $0.75$ , which roughly bound the velocity curve at all appreciable levels. The value of  $N = 0.25$  matches the slope of the numerical solution closely down to about 26 km. For lower altitudes it falls much too slowly. The value of  $0.75$  lies slightly below the numerical solution to about 25 km. For lower altitudes it is significantly higher, although that is a level such that little radiation would be produced.

It is clear from the form of Eq. (16) that if  $M$  increased or  $\rho$  decreased, the velocity at any time would decrease. The neglect of the erosion of  $M$  and of the increase of density during



deceleration has just that effect. Thus, it is expected that the analytic velocity would have larger values at late times. It is possible to use more careful approximations to  $M$  and more careful integrations over density to remove these errors. However, the goal here is to produce an invertible approximation for the power radiated during the maximum deceleration period, for which those corrections are not required. For the approximate velocity of Eq. (16), the approximate radiation rate is

$$P = \rho (D + V_t t)^2 V^3, \quad (17)$$

which is compared with the numerical result in Fig. 7. The numerical value is shown by the solid squares. The curve for  $N = 0.25$  lies well above it at peak, peaks at a lower altitude, and falls much more slowly at lower altitudes. The curve for  $N = 0.75$  peaks at the same altitude, although at a lower altitude, and falls about as rapidly at lower altitudes. Depending on whether it was necessary to model the peak power or integral energy, the curve for  $N = 0.75$  could be adjusted to the numerical result by multiplying the peak or integral by about a factor of  $4/3$ .

**Impactor parameters.** Using Eq. (1),  $P$  may be written as

$$P \propto y^2 / (y^3 + K)^3, \quad (18)$$

where  $y = D + V_t t$  and  $K = 3MV_t / NC_p f V_0 - D^3$ , whose solution is

$$D + V_t t = (2K/7)^{1/3}, \quad (19)$$

from which the time to <sup>reach</sup> maximum power is

$$t_{\max} = [(2K/7)^{1/3} - D] / V_t, \quad (20)$$

and the altitude to maximum power is

$$\Delta z_{\max} = V_0 t_{\max}, \quad (21)$$

which is shown in Fig. 8 for 0.5 and 1 m objects incident vertically at 15 km/s. The 1 m object travels about 3 km from a fragmentation at 35 km to peak radiation at 32 km. The 0.5 m object travels about 1.5 km. For fragmentation at 25 km, those distances are each about halved. The 1 m fragments would deposit at about  $25 - 1.5 = 23.5$  km, in accord with Fig. 7 for  $N = 0.75$ , which was also used in constructing Fig. 8. For fragmentation altitudes below 20 km the deposition altitudes are only about 1 km lower, which is probably not detectable.

Figure 9 shows the deceleration altitude of 0.5 and 1 m objects as functions of their initial velocity. The smaller objects decelerate higher, particularly at higher velocities. Figure 10 shows the time to peak radiation as a function of object size and speed. The larger objects have longer times because they penetrate further. The times to peak are short compared to the width of the peak radiation, but could be useful as auxiliary diagnostics.

**Inversion for fragmenting and ablating objects.** These results can also be used to work backwards to infer the parameters of fragmenting objects from observations. For fragmenting objects, the fundamental measurements are the peak power and altitude. From Eqs. (18) and (19),

$$P \propto y^2 / (y^3 + K)^3 = (2K/7)^{2/3} / (2K/7 + K)^3 \sim 1/K^{7/3}, \quad (22)$$

so that  $K \sim P^{3/7}$ , which can be used with Eq. (19) to estimate  $t$  and  $D$  as before. Thus, this solution for fragmenting and ablating objects maintains the invertibility of the earlier separate solutions for objects that fragmented or ablated only.

**Summary and conclusions.** This note discusses the estimate of the parameters of objects that both fragment and ablate during entry. It uses the kinematic results of previous reports to describe the velocity and pressure of entering objects. It shows that the mechanisms used to describe the breakup of non-ablating objects during deceleration remain valid for most ablating objects as well. It provides a more detailed treatment of the further breakup and separation of fragments during their descent. It replaces the constraint on mass per unit area used earlier to determine the altitude and magnitude of peak power radiation with a detailed analytic solution of their time dependent deceleration. This analytic model is shown to be sufficiently accurate and to reduce to those derived earlier in appropriate limits. The model predictions are shown to be in agreement with the key features of numerical calculations of deceleration—particularly velocity and power. The model equations are solved for the altitude of maximum radiation, which agrees with numerical integrations. The model is inverted analytically to infer object size and speed from measurements of peak power and altitude. It thus forms a complete model for the approximate inversion of meteor data.

## References

1. G. Canavan, "Radiation from Hard Objects," Los Alamos National Laboratory report LA-UR-97-662, February 1997.
2. G. Canavan, "Deceleration and Radiation of Strong, Hard, Asteroids During Atmospheric Impact," Los Alamos National Laboratory report LA-UR-95-1477, 1 Feb 1997.
3. G. Canavan, "Meteor Signature Interpretation," Los Alamos National Laboratory report LA-UR-97-128, January 1997.
4. G. Canavan, "Fragmentation of Weak Non-Ablating Objects During Entry," Los Alamos National Laboratory report LA-UR-97-, April 1997.
5. C. Chyba, P. Thomas, and K. Zahnle, "The 1908 Tunguska explosion: atmospheric disruption of a stony asteroid," *op. cit.*
6. G. Canavan, "Fragmentation of Weak Non-Ablating Objects During Entry," *op. cit.*
7. J. Hills "The Fragmentation of Small Asteroids in the Atmosphere," the *Astronomical Journal*, **105**, No. 3, March 1993, pp, 1114-1144.

v vs z compare

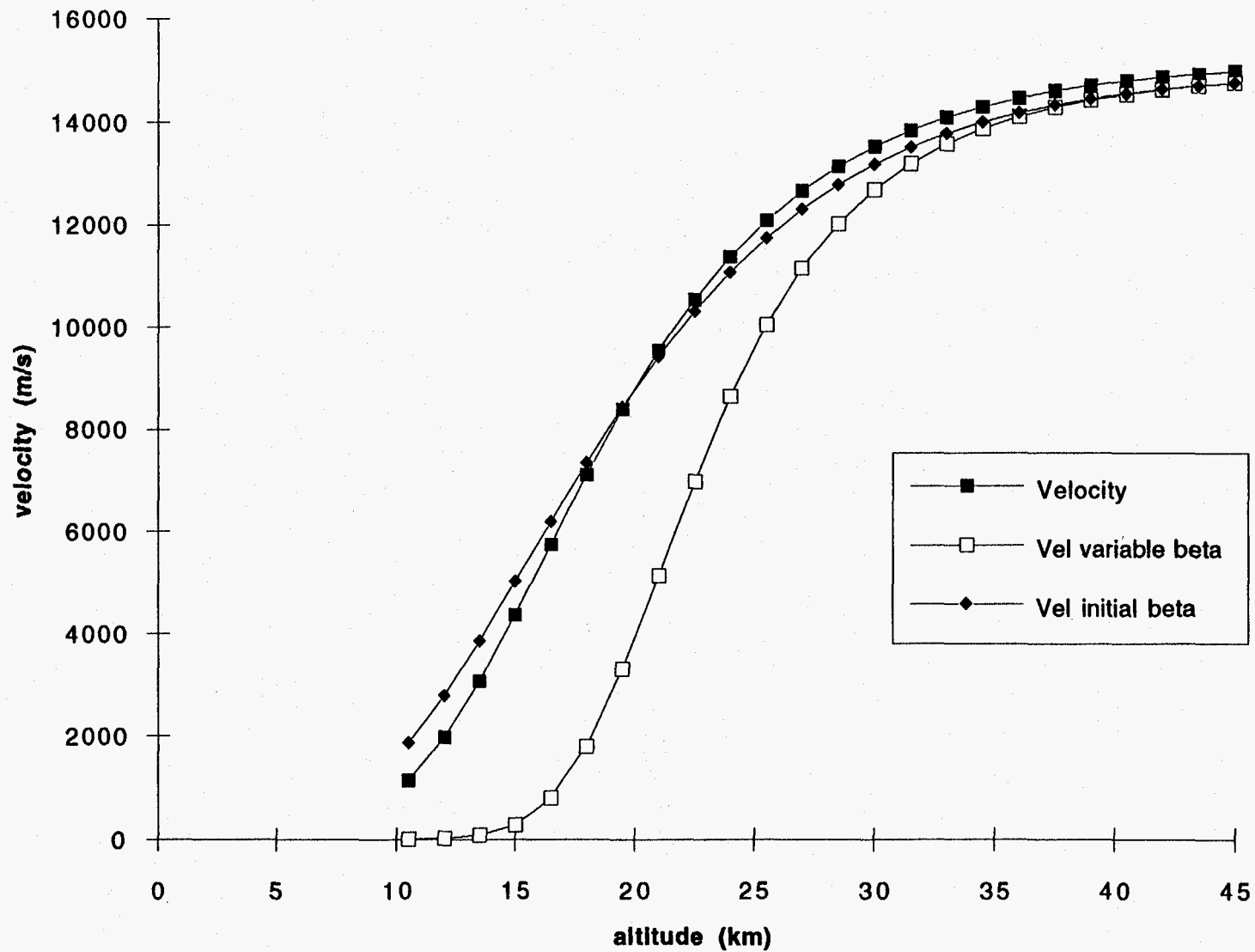


Fig. 1. Velocity versus altitude.

p vs z comparison

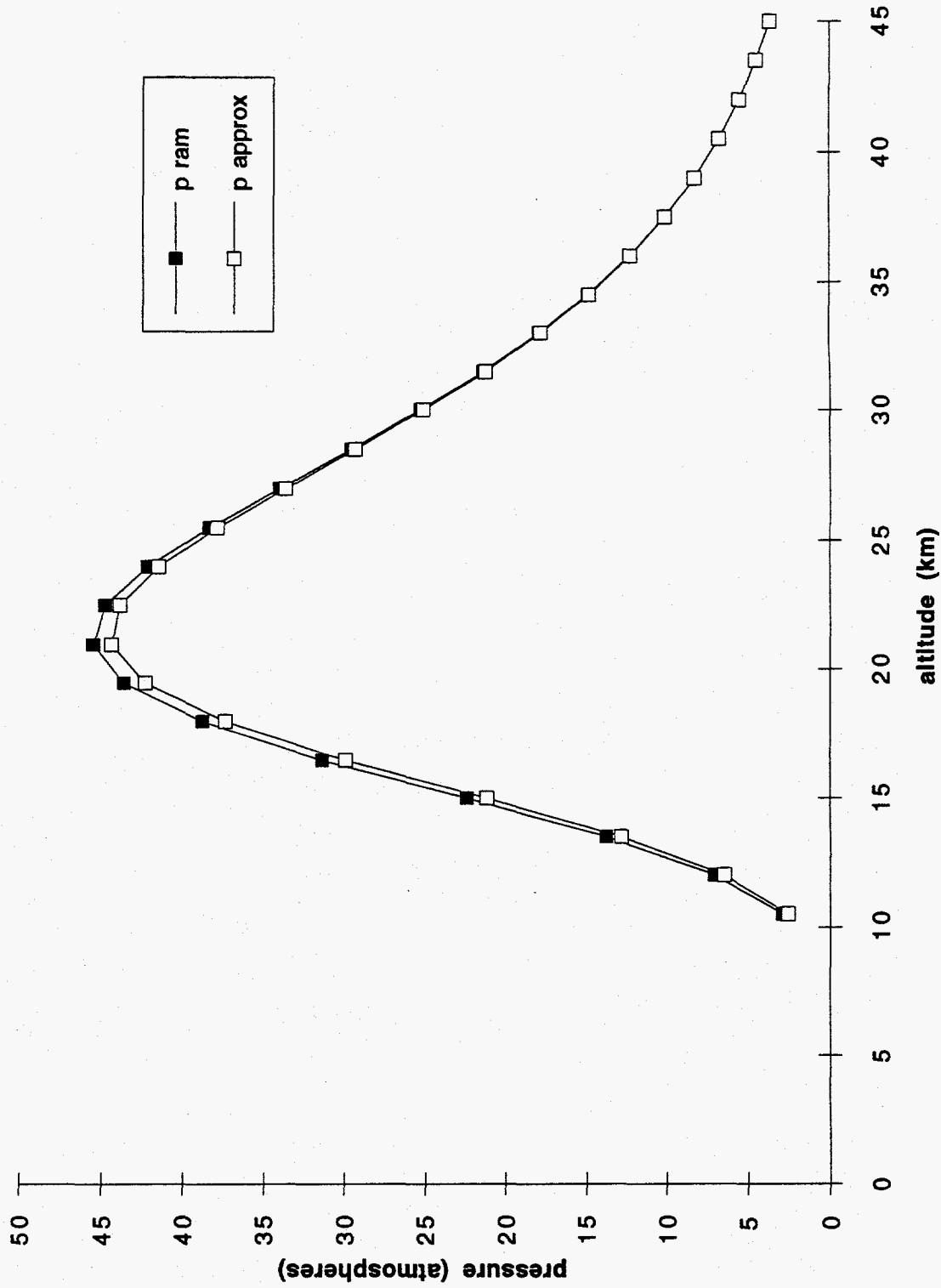


Fig. 2. Pressure--ram and approximate--vs altitude for 0.5 m object.

P vs z; Q 5

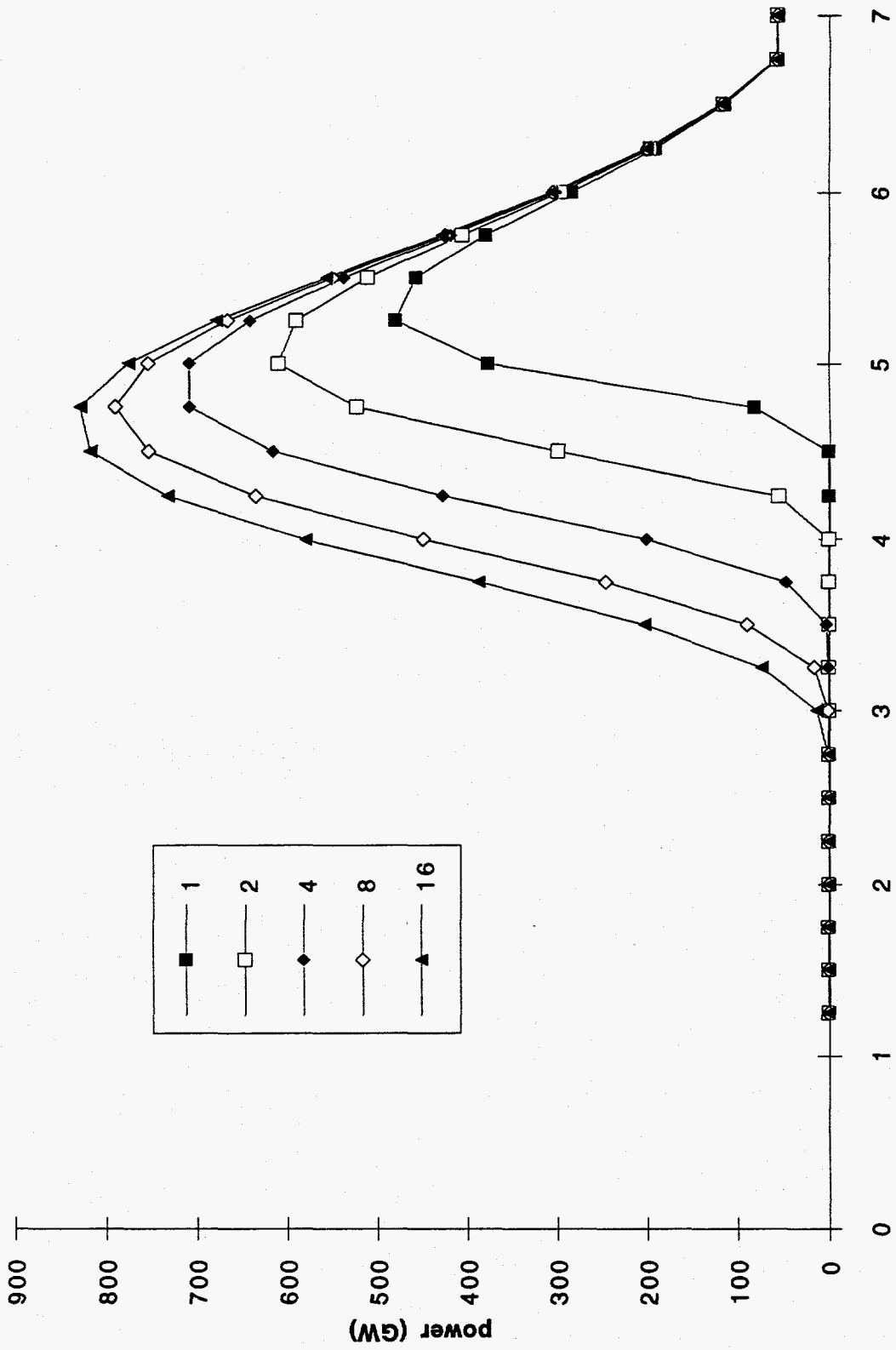


Fig. 3. Power after fragmentation for various heats of vaporization (MJ/kg).

V vs z; 5Q

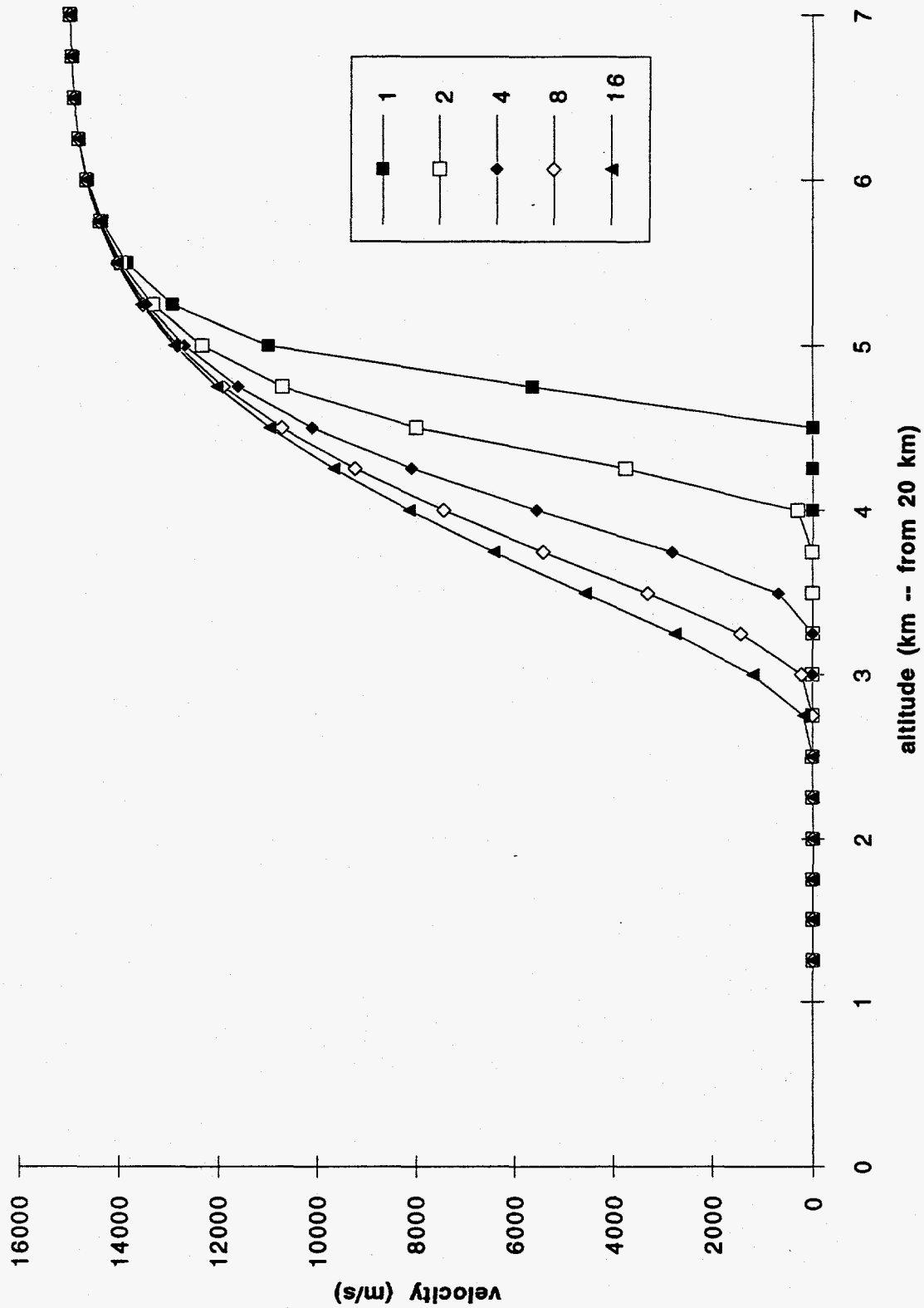


Fig. 4. Velocity versus altitude for 1 m objects at 15 km/s with various heats of vaporization (MJ/kg).

mass vs z; Q

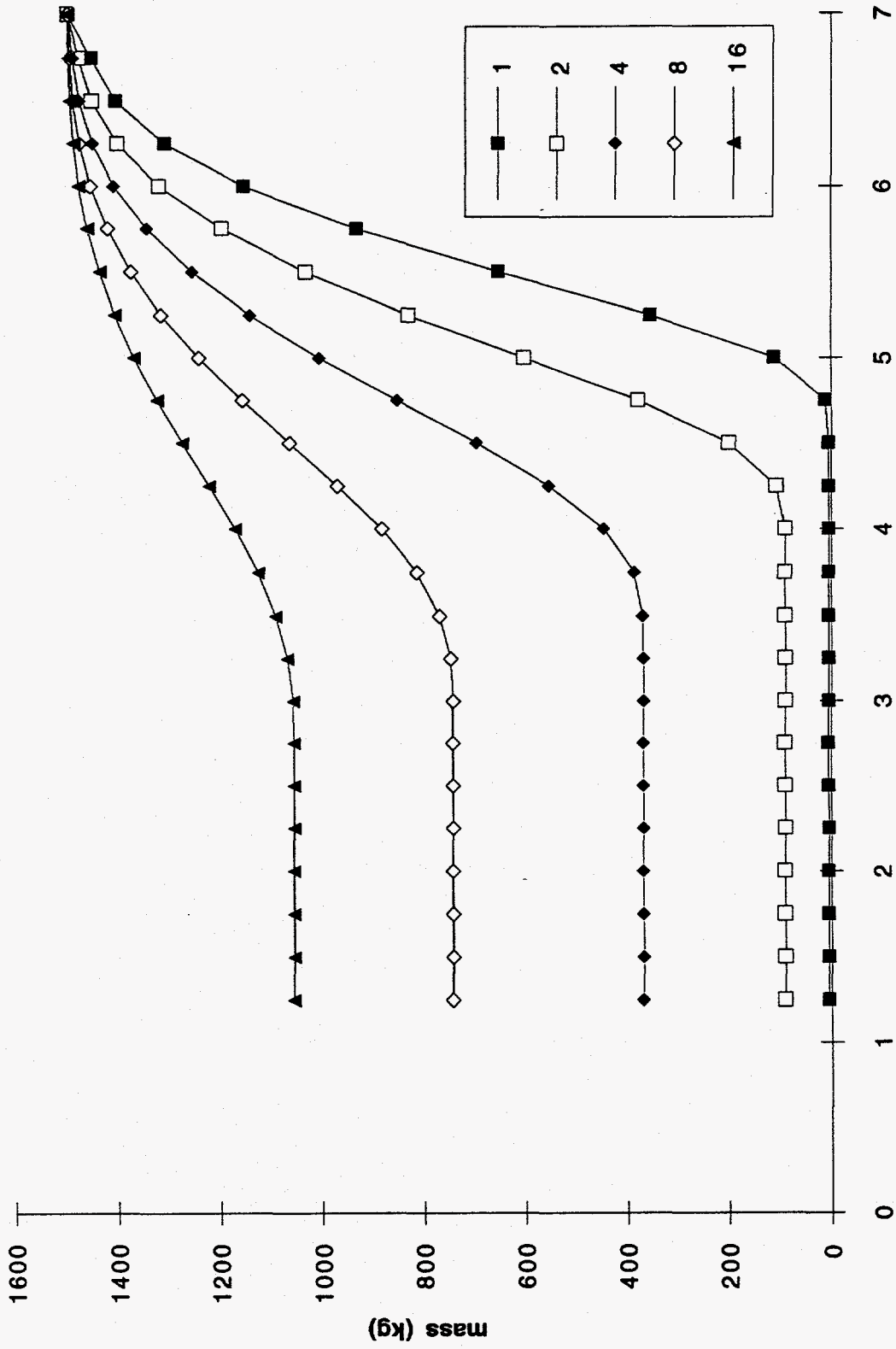


Fig. 5. Mass versus altitude for 1 m objects at 15 km/s with various heats of vaporization (MJ/kg).

comp num & approx V vs z

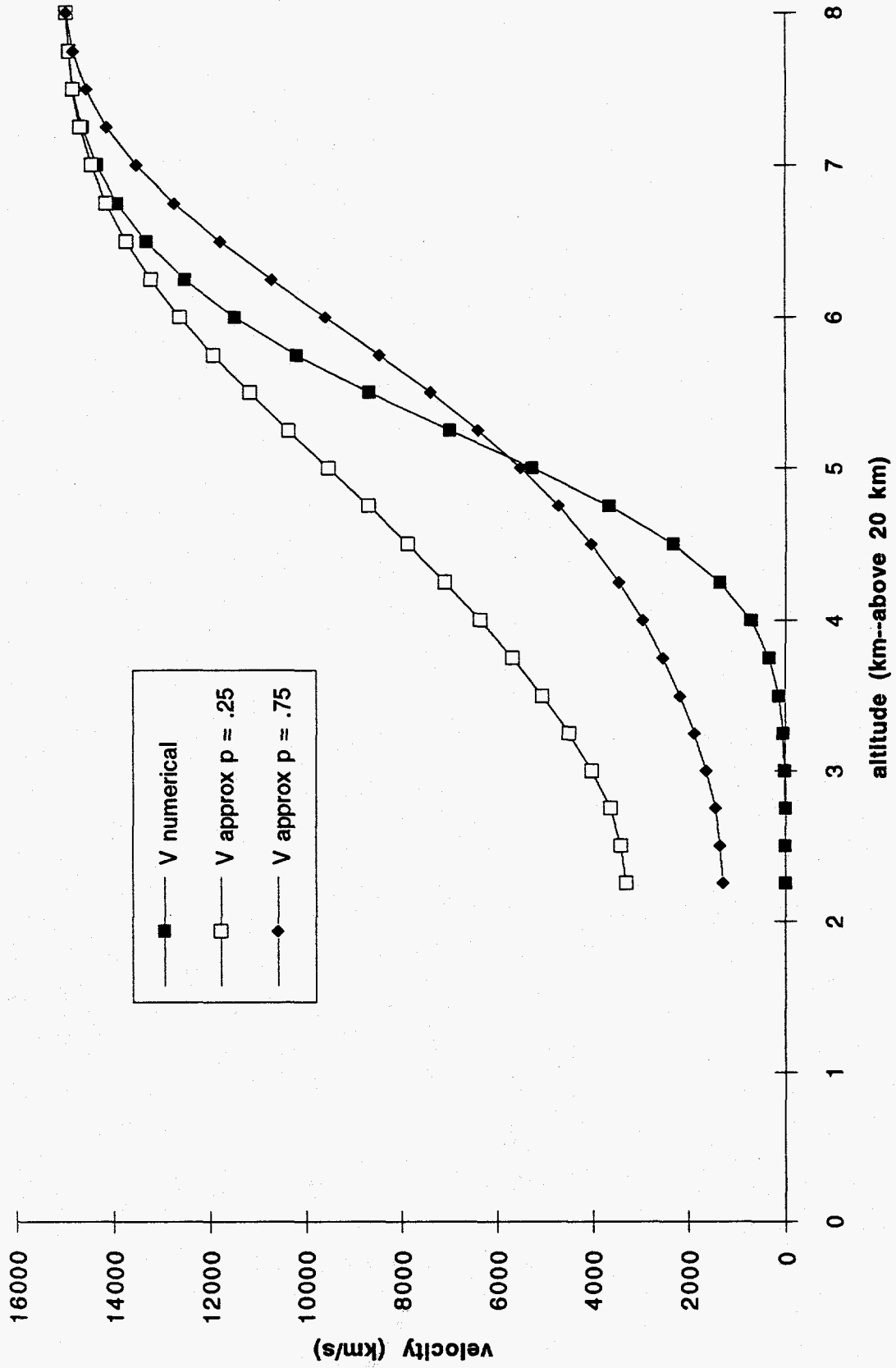


Fig. 6. Comparison of numerical and analytic velocities.



compare power vs alt 1 m

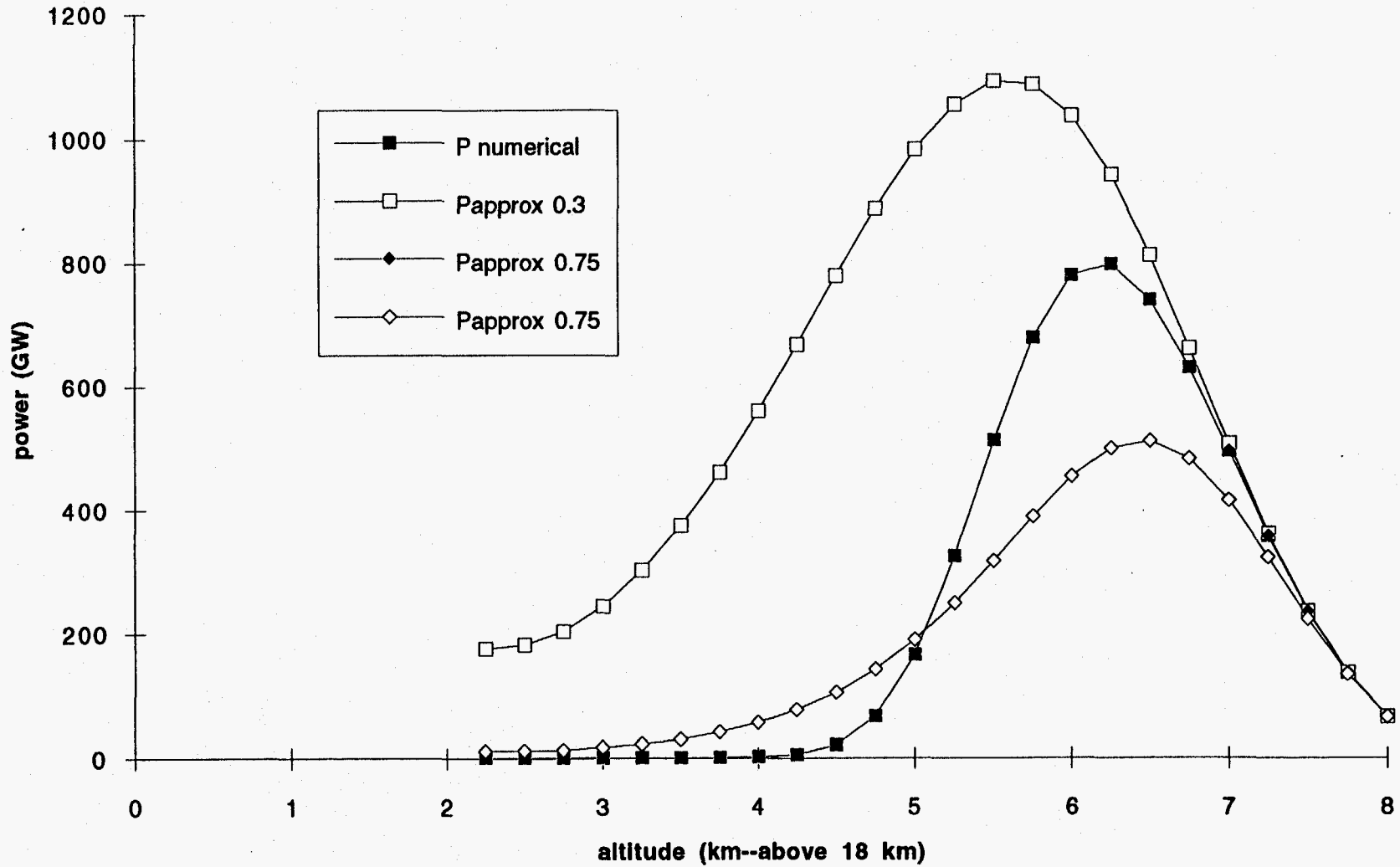


Fig. 7. Comparison of numerical and analytic power histories for 1 m fragmentation at 26 km.

distance to max vs frag alt

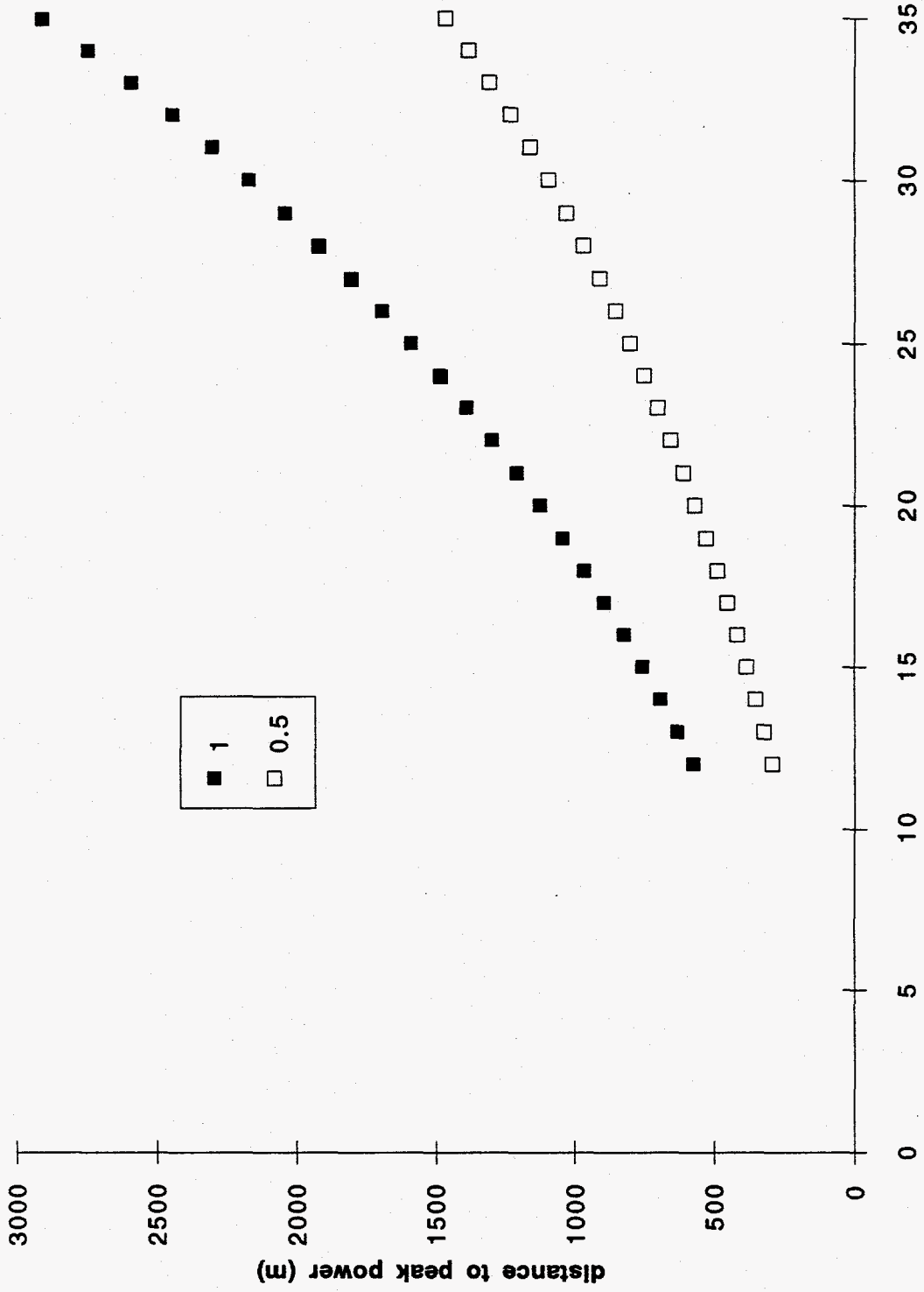


Fig. 8. Altitude from fragmentation to max power for various diameters (m).

decel alt vs Vo approx

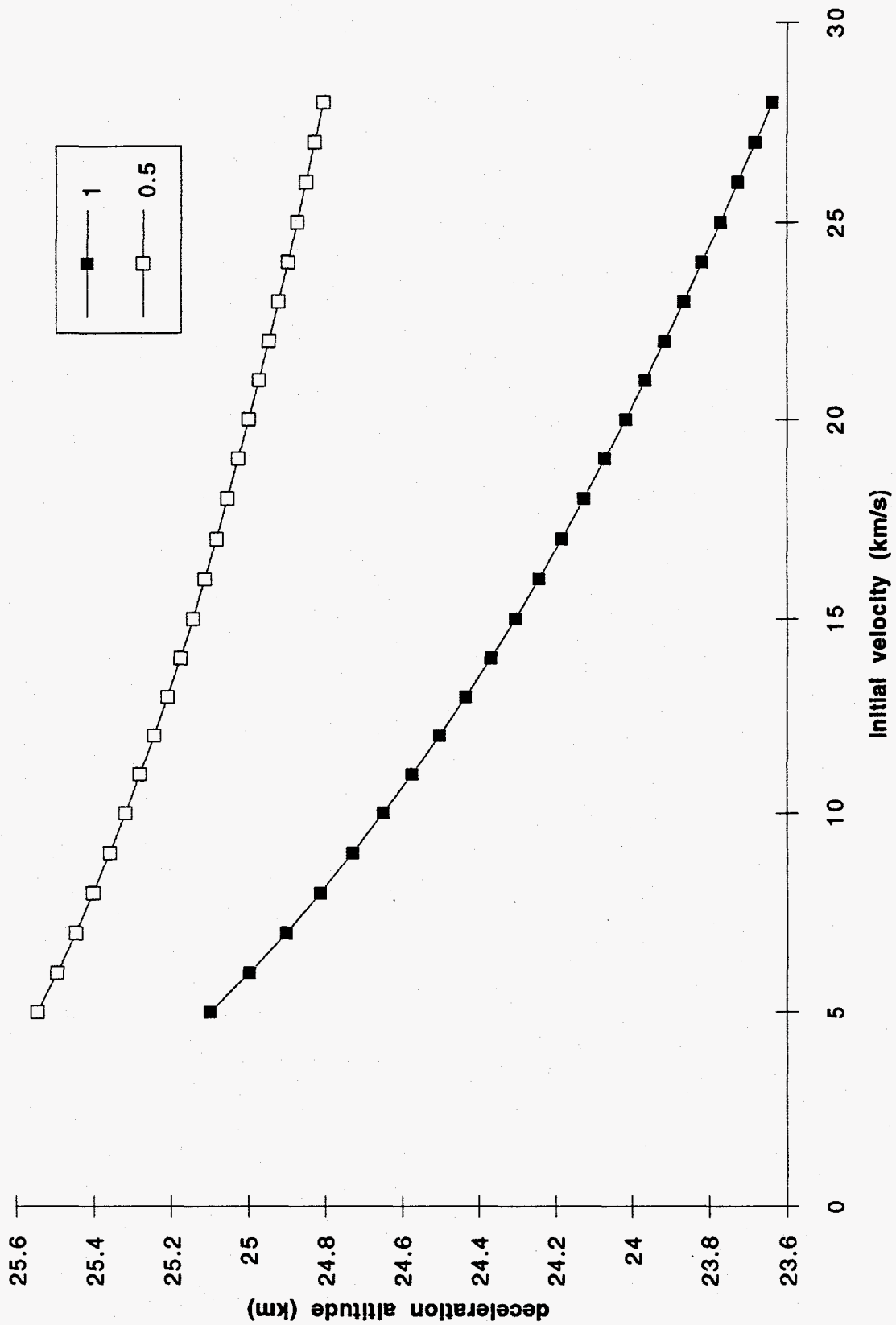


Fig. 9. Peak radiation altitude versus initial velocity for 26 km fragmentation of objects of various diameters (m).

time to peak rad vs  $V_0$

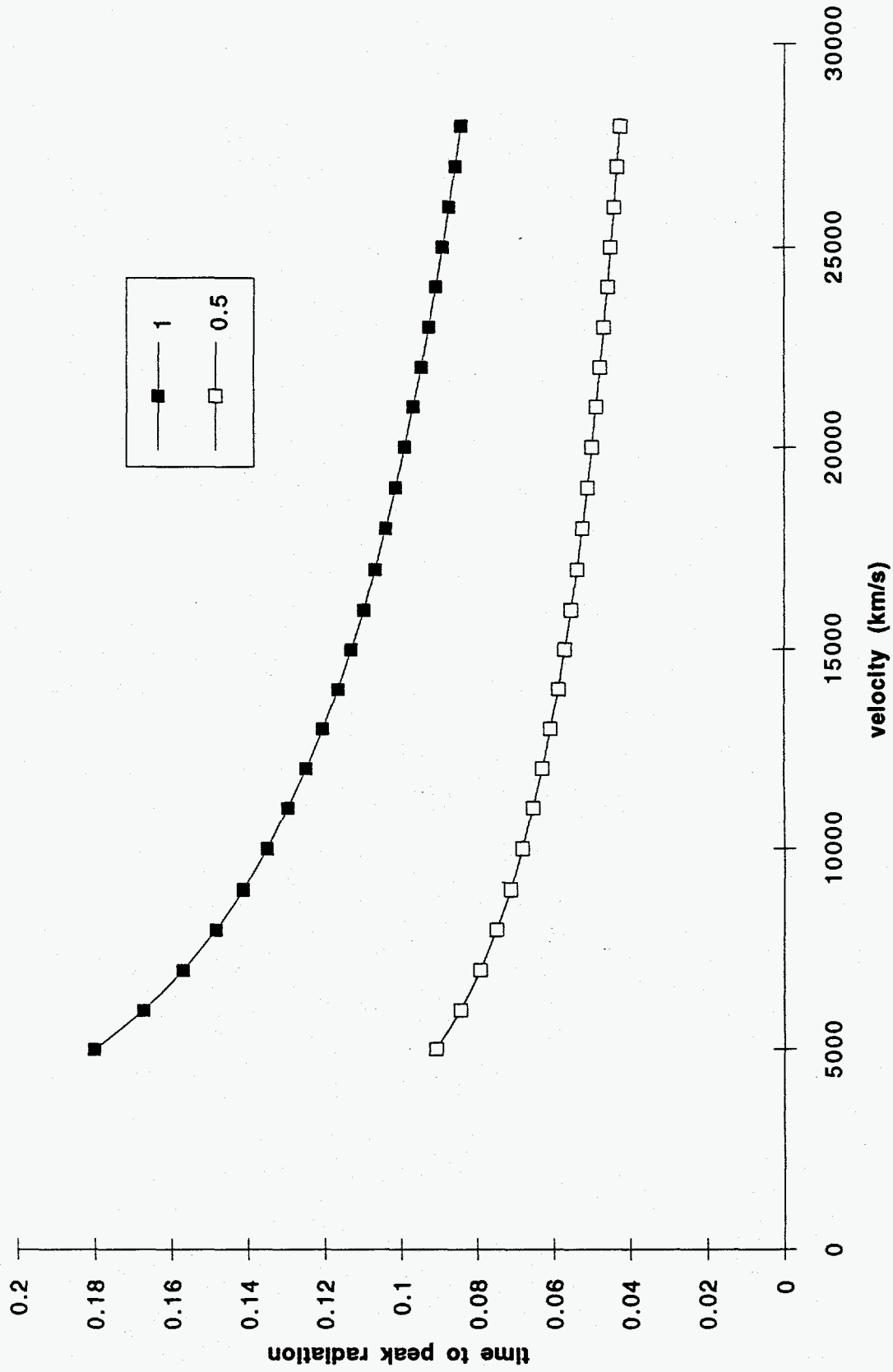


Fig. 10. Time to peak radiation vs velocity for various diameters.